small
NANO MICRO

Restructuring and Remodeling of $NaREF_4$ Nanocrystals by Electron Irradiation

Xiaoyu Sun, Bingru Wang, Ivan Kempson, Chunyan Liu, Yi Hou, and Mingyuan Gao**

***N**aREF$_4$ nanocrystals are found to be highly manipulable by electron beam irradiation. With 200 kV electron beam irradiation, both 14.6 nm spherical NaGdF$_4$:Yb,Er nanoparticles and 44.7 nm × 34.1 nm ellipsoidal NaYF$_4$:Yb,Er nanorods form hollow structures and eventually convert to the corresponding REF$_3$ upon prolonged irradiation. Furthermore, the NaYF$_4$ nanorods fractured with irradiation with a 100 kV electron source are found to be subsequently self-healed when irradiated with a 200 kV source. The detailed experimental results, in combination with theoretical analysis, suggest that knock-on effects, specific lattice energy, and the inherently low surface energy of NaREF$_4$ collectively contribute to the formation of the hollow structures. These mechanisms allow controlled engineering and manipulation of RE nanomaterials on the nanometer scale.*

1. Introduction

Energetic particle interactions with solid materials have been studied for several decades in particular interest of nuclear and space technologies. Only in more recent years however, have these interactions been explored for beneficial outcomes with respect to atomic level processes and structures.

Simultaneously, the interactions of a beam of electrons with materials have also been intensively investigated, laying solid foundations for transmission electron microscopy (TEM) coupled with various imaging and structural analyses based on the varying nature of electron interactions with matter. However the occurrence of radiation damage induced by the electron beam is often observed while imaging. For example, it has been reported that nanomaterials, such as Au nanoparticles,[1] metal oxide nanoparticles,[2] silicon oxide nanowires,[3] and lead iodide nanoparticles[4] undergo structural changes under electron beam irradiation. Although typically regarded as detrimental, the radiation damage by electron beams also offers opportunities for manipulation and even fabrication of interesting nanostructures.[5,6]

Energy transfer during electron irradiation proceeds by two paths: electronic interactions or nuclear (knock-on) collisions.[7] Electronic interactions transfer energy from the incident electron to the electrons in the specimen, resulting in a variety of phenomena including plasmon, phonon, excitation and ionization processes. Knock-on collisions involve the interaction of the incident electron with an atoms nucleus. If the transferred energy is greater than the displacement threshold energy, the atom can be displaced to become an interstitial or be ejected.[8,9] These processes can act in a detrimental way, significantly degrading structural properties and stability of materials, however in the field of nanoscience avail exciting opportunities in fabrication, atomic manipulation, and fundamental study of structure and self-healing properties in nanometer scales. Understanding the occurrence and evolution of material restructuring induced by electron irradiation is therefore of both scientific and technical importance for developing advanced materials.

Ability to preferentially encourage specific mechanisms is exemplified by the publication of Wu et al.,[6] whereby stable voids were produced in sheets of Mg via the knock-on effect by a high current density, 200 kV electron beam. However with low current density, the electron beam irradiation then led to self-healing of the void, with Mg atoms reconfiguring to reduce the void size until it disappeared.

Furthermore, while spatial confinement on the nanoscale is greatly appreciated for properties imparted

X. Y. Sun, B. Wang, Dr. I. Kempson,[+] Dr. C. Liu, Prof. Y. Hou, Prof. M. Y. Gao
Institute of Chemistry
the Chinese Academy of Sciences
Bei Yi Jie 2, Zhong Guan Cun
Beijing 100190, China
E-mail: houyi@iccas.ac.cn; gaomy@iccas.ac.cn
[+]Present address: Ian Wark Research Institute, University of South Australia, Mawson Lakes, S.A. 5095, Australia

DOI: 10.1002/smll.201401101

to photon-matter interactions, comparatively little has been described for electron-matter interactions. Strains, stresses, and the ability for phonon transport also depend on nanoscale confinement/structure that diverge from bulk or perfect crystal material properties and contribute to physico-chemical,[10] mechanical,[11] energy transfer and thermal behavior.[12] Additionally, nanocrystals may possess defects within their lattice, or they can be induced from electron irradiation which imparts further manipulation of nanocrystal structure. Defects can contribute to optical-nanoparticle interactions,[13] and magnetic properties,[14] likewise they impart a reduction in lattice energy that facilitates localized plasticity. Understanding the role of defects in nanoparticles and their study however, is particularly challenging.[15] Likewise, with regard to carbon nanostructures, Banhart indeed stated that nanoparticle structures in a thermodynamically unfavourable state resulting from electron irradiation cannot be explained by simple structure models only, requiring new concepts yet to be developed.[16]

Herein, we report our observations of structural remodelling, crystallographic conversion and self-healing of hexagonal $NaREF_4$ nanoparticles induced by electron irradiation. The hexagonal $NaREF_4$ nanocrystals were chosen as a model to investigate the irradiation damage of rare earth crystals which have utility for their optical properties,[17–21] while hollow $NaREF_4$ nanoparticles have established promise as drug carriers.[22,23] The mechanisms of the structural evolutions of $NaREF_4$ nanocrystals are also discussed.

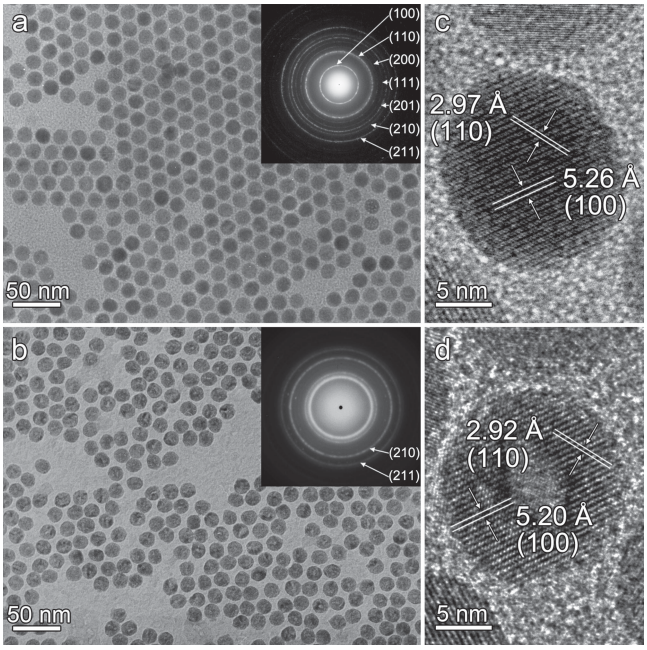

Figure 1. TEM images of $NaGdF_4$:Yb,Er nanoparticles a) before and b) after electron beam irradiation for 10 min with 100 kV electron acceleration voltage, insets of (a,b) show the corresponding SAED patterns labelled with Miller indices according to hexagonal phase $NaGdF_4$ (JCPDS 27–0699). HRTEM images of $NaGdF_4$:Yb,Er nanoparticles c) before and d) after electron beam irradiation with 200 kV electron accelerating voltage, overlaid with crystal plane identifications.

2. Results and Discussion

A typical structural reconfiguration of $NaGdF_4$:Yb,Er nanocrystals (14.6 ± 0.7 nm) induced by electron beam irradiation in TEM (100 kV) is shown in **Figure 1**. The $NaGdF_4$:Yb,Er particles present normal contrast of solid particles upon quick imaging (Figure 1a). However, prolonged exposure time (10 min) leads to cracks occurring in the $NaGdF_4$:Yb,Er particles (Figure 1b). Careful high resolution TEM (HRTEM) measurements suggest that the prolonged electron beam irradiation produced what appears as a hollow shell structure (Figure 1d). Lattice fringes in the bright central region lost contrast, while those in the outmost part remain clearly defined, contrasting to a fresh particle quickly imaged by HRTEM at 200 kV (Figure 1c). A small reduction in lattice plane spacing presented by HRTEM measurements further indicates some structural changes taking place as a result of the electron beam irradiation. The analysis of the interplanar distances revealed that the outermost part of the nanoparticles remains as a hexagonal structure. The selected area electron diffraction (SAED) results, given as insets in Figure 1a and 1b, further reveal that prior to irradiation the nanocrystals exhibit 7 diffraction rings attributable to hexagonal $NaGdF_4$, while only 2 remain after irradiation.

To study the structural reconfiguration as a function of time, HRTEM images were taken from a small group of nanoparticles over the course of 720 seconds in the electron beam accelerated by 200 kV voltage (**Figure 2**a–e). Small voids appear within the first 1–2 min which subsequently enlarge and coalesce, resulting in hollow particles. Figure 2f shows that the particle outer diameter remains nearly unchanged over this time frame. To confirm the resulting structure was indeed hollow, TEM images were acquired through a tilt series from 0 to 30°. As shown in **Figure 3**a, the shape and size of the morphological features remain almost unchanged. Further simulation of the contrast changes upon titled angle for particles bearing hollow, cylindrical, and bowl-shaped defects, respectively, are shown in Figure 3b–d. Only the hollow sphere configuration matches the TEM observations, as shown in Figure 3b.

In fact, similar transformation of a solid $NaREF_4$ nanocrystal to hollow particle was previously observed by Feng et al.[24] However this process was not accompanied by any observed crystal structural change. They hypothesised an electron beam lithographic process preferentially ablated material, via localized heating, from $NaREF_4$ nanocrystals comprising aggregated organic matter used in the nanoparticle synthesis which had become encapsulated in the nanocrystal. The encapsulation of organic materials in inorganic crystalline structure challenges the conventional mechanisms of crystal growth, and on the other hand would lead to observable contrast variations across the crystal due to presence of aggregates of low Z composition within the nanocrystals. However, it is difficult to find such evidence from the HRTEM image shown in Figure 1c. Therefore the following characterization was carried out to verify their hypothesis and reveal the underlying mechanisms of the current observations.

Energy dispersive X-ray (EDX) analysis was firstly performed to investigate the composition change in an individual

NANO MICRO small

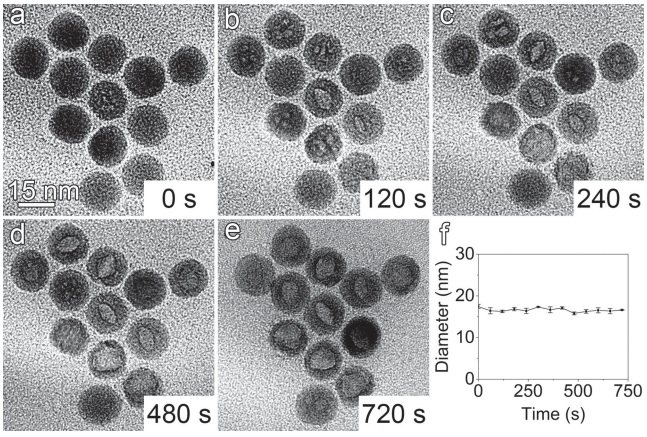

Figure 2. a–e) Time dependent reconfiguration of $NaGdF_4$:Yb,Er nanoparticles induced by 200 kV electron beam irradiation, together with f) the overall time dependent diameter of the particles over the irradiation process.

nanocrystal before and after the structural evolution. The results in **Table 1** as well as Figure S1 in Supporting Information (SI) reveal that the content of F, measured with the beam being focused on the center of the particle, decreases greatly after 10 min irradiation, whereas the contents of the rest of the elements increase. This strongly indicates that light elements such as F were knocked out of the crystal by electron beam irradiation. By assuming that the ejection of Yb was minimal as it is the heaviest element in the particle, discussed in more detail below, the atomic ratios of the rest of the elements were normalized with reference to Yb and

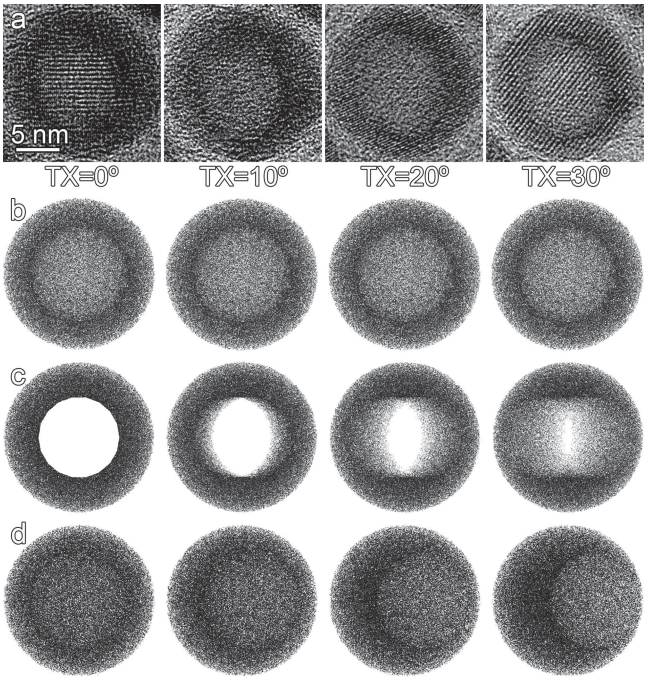

Figure 3. a) TEM images of a $NaGdF_4$:Yb,Er nanoparticle observed with tilting angles of 0 to 30 degrees. b–d) Projection images of three spherical particle models with a hollow core (b), cylindrical (c), or bowl-shaped void (d), viewed by the same tilting angles.

Table 1. Elemental composition of an individual nanocrystal before and after electron beam irradiation for 10 min.

Element	Atomic mass	Before [%]	After [%]	Before*	After*
F	19.0	52.15	19.21	9.73	1.98
Na	23.0	4.68	6.97	0.87	0.72
Gd	157.3	34.86	58.80	6.50	6.06
Er	167.3	2.94	5.32	0.55	0.55
Yb	173.0	5.36	9.70	1.00	1.00

*Normalized with reference to Yb content.

listed aside. According to the normalized data, F atoms are heavily lost during electron beam irradiation, followed by Na. Only a small loss is presented with respect to Gd that is the third heaviest element. Note that the EDX analysis spectra were acquired for 1 minute and structural alteration of the particles was occurring within this time; hence the composition measured did not reflect the true initial stoichiometric composition. However, EDX analysis reveals the particles are losing F and Na faster than losing RE atoms under electron beam irradiation. Point-by-point analysis of Gd across a single particle (Figure S2 in SI), while having low signal to noise ratio, reveals that Gd atoms are preferentially re-distributed at the particle edge upon irradiation, suggesting that the ejection of light elements leaves a hollow structure and a shell rich in RE elements behind. After exhaustive irradiation of 40 min, the crystal was transformed principally into GdF_3, supported by the SAED pattern shown in Figure S3 in SI. The diffraction patterns however indicate a 100% conversion has not been achieved and remnants of the original structure persist. By assuming that $NaGdF_4$ (density = 5.65 g cm^{-3}) is completely converted to GdF_3 (7.06 g cm^{-3}) by losing Na and F, the volume reduction is calculated to be approximately 33% according to their densities. Thus, the maximum diameter of the void in a 15.7 nm nanosphere would then be expected to be ≈ 10.9 nm, slightly larger than the actual size of the voids shown in Figure 3 due to the fact that 100% conversion was not achieved. Nevertheless, all these results suggest new mechanisms different from previously proposed mechanistic concepts.[24]

According to the EDX results, Na and F are significantly and preferentially lost from the nanocrystals upon electron beam irradiation. The interactions between the energetic electrons with atoms' nuclei are discussed below. In theory, these interactions can be treated as an elastic two-body collision as shown in Figure S4 in SI. Because the mass of the atom is much greater than the electron, the acquired momentum of an atom in the collision can be expressed by

$$P = 2\sin\left(\frac{\theta}{2}\right)P_0 \quad (1)$$

where P_0 is the momentum of the electron before the collision and calculated from

$$E_T^2 = (m_0c^2 + E_1)^2 = E_1^2 + P_0^2c^2 \quad (2)$$

where E_T and E_1 represent the total energy and kinetic energy of electron, respectively; m_0 is the rest mass of an electron and c, the velocity of light. Therefore, the maximum acquired kinetic energy (E_{max}) of an atom in the elastic collision is

$$E_{max} = \frac{P^2}{2M} = \frac{2E_1(2m_0c^2 + E_1)}{Mc^2} \quad (3)$$

where M is the mass of the atom. As shown, E_{max} is inversely proportional to M under constant accelerating voltage, so E_{max} for a fluoride atom is at least 8 times higher than that for rare earth atoms in the current system. For example, under a 100 keV electron beam, E_{max} is 12.7 eV for F, 10.5 eV for Na, and 1.5 eV for Gd; while under a 200 keV electron beam, E_{max} becomes 27.6 eV for F, 22.8 eV for Na, and 3.3 eV for Gd. Therefore, it is reasonable to expect that the light atoms are much easier to be ejected out of the solid sample upon electron beam irradiation as they acquire much higher kinetic energy. Nevertheless, the displacement or ejection of atoms is also strongly associated with their binding energy.

The lattice energy (U_{pot}) for a hexagonal $NaGdF_4$ crystal can be expressed by Equations 4,5:[25]

$$I = \frac{1}{2}\sum n_i z_i^2 \quad (4)$$

where I is defined as the ionic strength-like term, in which n_i is the number of ions of type i per formula unit, z_i represents the valence of i type ion. The lattice energy, U_{pot} can be written as

$$U_{pot} = 2I(\alpha V_m^{-1/3} + \beta) \quad (5)$$

where V_m is the volume per formula unit, α (138.7 kJ mol^{-1} nm) and β (27.6 kJ mol^{-1}) are coefficients for $NaGdF_4$ from the best fits. According to Equations 4,5, U_{pot} of a hexagonal $NaGdF_4$ crystal is about 4985 kJ mol^{-1}, and thus the average lattice energy for a $NaGdF_4$ unit cell is ≈ 77.6 eV, and the binding energy of F^- is around 12.9 eV on average. According to literature data of U_{pot} for GdF_3 (5122 kJ mol^{-1})[26] and NaF (910 kJ mol^{-1}),[25] the binding energy of F^- in the GdF_3 and NaF unit cells is approximately 17.7 eV and 1.2 eV, respectively, which suggests that $NaGdF_4$ is much more stable than NaF, but less stable than GdF_3 under electron beam irradiation. In other words, $NaGdF_4$ can be converted into GdF_3 by proper selection of the incident energy of electrons initiated by knock-on effects. A high surface area to volume ratio typical of nanoparticles facilitates F^- ejection.

Furthermore, by combing the above theoretical analyses, it is reasonable to expect that rare-earth elements in the particle system are difficult to be ejected because on the one hand it receives much lower kinetic energy, and on the other hand they possess much higher binding energy due to a greater coordination. Therefore, the RE elements have to be heavily displaced under the irradiation so as to form a hollow structure.

In principle, electron-nucleus interactions will only be observable if the displacement threshold energy is exceeded. According to the above discussion, the energies used here are expected to be able to knock the low Z atomic species out of the particles. Due to the heavy loss of F^- ions, the resulting F vacancies as defects provide localized reduction in displacement threshold energy for RE elements, which facilitates the formation of small voids shown in Figure 2a,b. The small voids tend to merge to form a large one, probably driven by free energy of the system. With conduction of the light elements, and either spontaneous recombination of Frenkel pairs in the outer shell region or an intrinsic increase in defect concentration near the nanocrystal center, void growth becomes preferential. In consequence, a hollow structure with the finally formed void being closer to the nanoparticle centre is generated (Figure 2). The preferential process of void growth and coalescence resulting in the hollow structure rather than a volume contraction can be explained by a balance driven by thermodynamic preference for reduction of the total surface energy of the void (lowering Gibbs free energy), with a lattice strength and associated forces/energies greater than the crystals surface energy, maintaining the outer shell dimension.

To provide more experimental evidence on the displacement of RE elements during irradiation, $NaYF_4$:Yb,Er particles were adopted as they presented a similar hollow structure under electron beam irradiation.[24] But different from the prior investigations, we herein chose axisymmetric ellipsoidal $NaYF_4$:Yb,Er nanorods with larger dimensions, that is, (44.7 ± 1.8) × (34.1 ± 2.2) nm, for showing more detailed effects.

Similar to literature results, the $NaYF_4$:Yb,Er nanorods can also form hollow structures by a 200 kV electron source (supported by the results and simulation in Figure S5). The evolution of the nanorods from a solid to hollow form was carefully recorded and shown in Movie 1 in the SI, while representative frames for exhibiting the structural evolution are provided in **Figure 4**. Similar to the spherical counterpart, the ellipsoidal nanorod also presents small voids that grow and coalesce against time, eventually giving rise to a large hollow structure. The fast Fourier transform (FFT) of these frames shown as insets of Figure 4a–d indicate a progressing structural transition after 4-min irradiation, while 10-min indicates an almost entirely converted crystalline structure. Further HRTEM analysis reveals that the initial morphological change is partly correlated with a gradual decrease in lattice distance of the (100) planes. Prolonged irradiation results in the conversion of $NaYF_4$ to YF_3, supported by SAED analysis provided in Figure S6. The conversion of $NaYF_4$ to YF_3 is faster than that of $NaGdF_4$ to GdF_3. This can be attributed to the difference in atomic mass of Gd (157.3) and Y (88.91) and the respective lattice energies. According to Equation 3, E_{max} for Y is almost twice that for Gd. Furthermore, the lattice energy for $NaYF_4$ (4457 kJ/mol) is smaller than that for $NaGdF_4$. Very interestingly, the fringes around the small voids start to exhibit curl and dislocations against time as shown in the insets of Figure 4b,c. Dislocations offer a mechanism for slip and plasticity, providing a means for atomic rearrangement that requires much less energy than otherwise required to restructure or break a crystal lattice.

NANO MICRO small

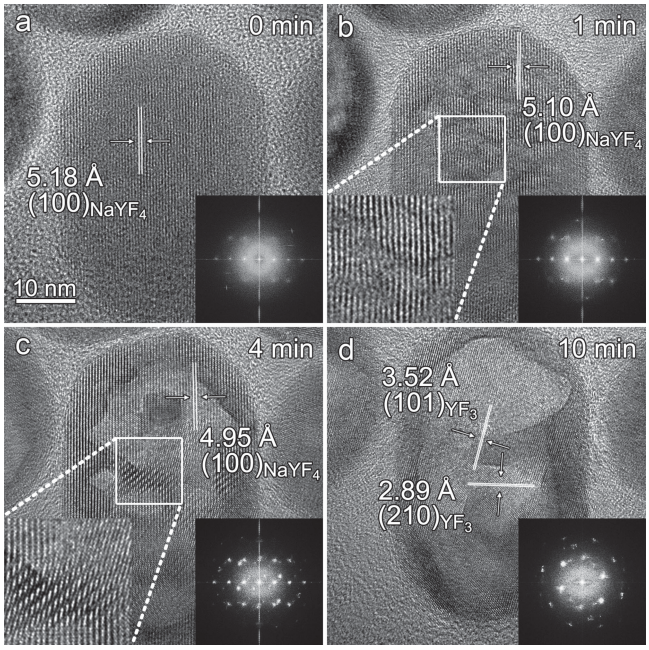

Figure 4. a–d) Time dependent reconfiguration of a $NaYF_4$:Yb,Er nanorod induced by 200 kV electron beam irradiation. Insets in the right corners are the FFT patterns, and the insets in the left corners of (b,c) are the enlarged images highlighted by the squares.

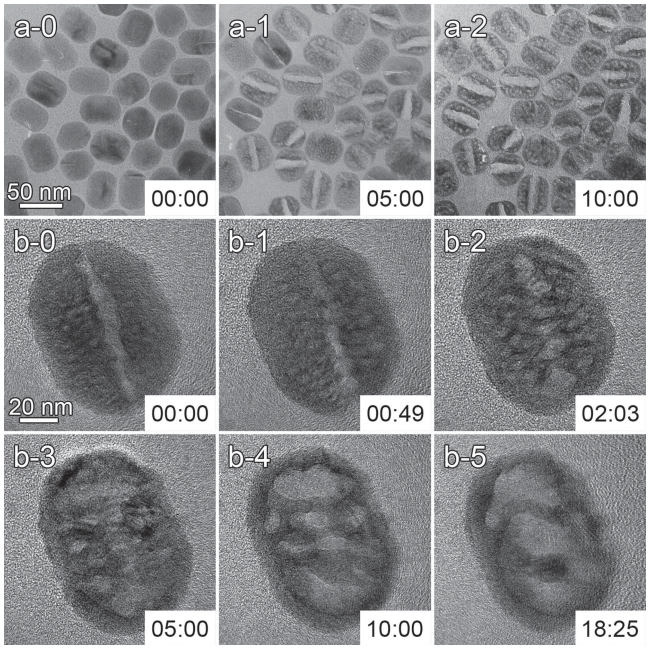

Figure 5. a) Time dependent fracturing of $NaYF_4$:Yb,Er nanorods induced by 100 kV electron beam irradiation. b) Time dependent restructuring of a fractured nanorod induced by 200 kV electron beam.

Zhu et al. observed a surface-extruded plastic flow and surface migration of atoms for 45 nm thick amorphous SiO_x nanowires. The existing knock-on mechanism and simulation were inadequate to explain their observations and they proposed an instability of atomic vibrations to control the processes. Moreover, they further demonstrated that the flow of atoms resulting in the extrusion was not caused by the local heating effect.[3] The flow observation can be expected to be more pronounced in amorphous material, compared to crystalline material, due to possessing a lower potential barrier for the mobility of atoms and higher surface energies. Regarding the flow of metal atoms in crystals, Wang et al. observed a 3–6 nm thickening of an oxide layer on a 100 nm Fe crystal core after 1 hour irradiation by electron beam accelerated by 200 kV. A beam activated mass transport rather than heating was also proposed for the structural transformation.[27]

Nevertheless, all the aforementioned structural changes occurring in the nanorods at 200 kV were not observed under 100 kV electron beam irradiation, unlike the situation for spherical particles reported in literature.[24] Instead, a fracturing phenomenon becomes dominant, apart from the formation of tiny void defects as shown in the upper panel of **Figure 5**. The nature of the fracture indicates a tensile stress normal to the crack. According to conventional theory, the force required would be significant as this process produces a considerably increased surface area and correspondingly increases the surface energy. However, based on the models of Xiong et al., we do not expect that nanostructured materials will behave physically similar to bulk material and can anticipate a reduction in surface energy at nanoscales.[28] Nevertheless, we have not had similar observations with non-$NaREF_4$ crystals and expect this behaviour stems from a low surface energy of $NaREF_4$ material relative to the elastic energy, hence the fracture can thermodynamically propagate. The propagation direction of the crack is anticipated to occur along the longitudinal axis (<001>) due to the fact that there are fewer number of bonds bridging unit cells perpendicular to this direction. With regard to fracture propagation, testing a nanoparticle to be ductile or brittle is challenging along with anticipating the plasticity around flaws. Conventionally, this observation suggests the nanoparticle to be brittle in nature and crack propagation occurs spontaneously.

Quite unexpectedly, irradiation of the fractured nanoparticles by 200 kV electrons subsequently leads to further plastic reorganization. As shown in the lower panel of Figure 5, the fracture actually bridges and reconfigures to revert to a hollow structure with prolonged irradiation time. A more detailed progression is provided in Movie 2 in SI. This remarkable self-assembly process into a hollow structure is far from being intuitive, but at least strongly supports that the heavy displacement of RE elements induced by electron beam irradiation can even enable plastic flow of RE atoms. This provides direct experimental evidence for understanding the formation of the hollow structures reported herein. The healing process for the fracture structure, converse to the 100 kV scenario where crack propagation was promoted, is probably caused by outward radial flow of all atoms involved. Presumably, RE elements do not gain enough energy to be ejected, they tend to form bridges across the gap, which is supported by the fact the spherical $NaGdF_4$:Yb,Er particle presents constant particle size through the electron beam irradiation (Figure 2d).

3. Conclusions

In summary, electron beam irradiation induced hollow $NaREF_4$ nanoparticles and the reconfiguration was carefully investigated. Systematic studies in combination with theoretical analysis suggest that knock-on effects, specific lattice energy and the inherently low surface energy feature of $NaREF_4$ collectively contribute to the formation of hollow nanocrystals. In addition, multiple processes including electronic excitations and ionic conduction (mobility of involved ions) are also involved in the morphological evolution. Identification and control of the discrete processes is currently challenging but will enable design and fabrication of advanced RE-based nanomaterials. Developing the basic understanding of material's deformation at the nanoscale will also be helpful for developing self-healing materials.

4. Experimental Section

Materials: $GdCl_3{\cdot}6H_2O$ (450855), $YCl_3{\cdot}6H_2O$ (211648), $YbCl_3{\cdot}6H_2O$ (337927), $ErCl_3{\cdot}6H_2O$ (259256), oleic acid (OA, 364525), octadecene (ODE, O806), and ammonium fluoride (NH_4F, 216011) were purchased from Sigma-Aldrich. NaOH, methanol, ethanol and cyclohexane were purchased from Sinopharm Chemical Reagent Beijing, Co., Ltd.

Preparation of $NaREF_4$ Nanoparticles: The syntheses of $NaREF_4$ nanocrystals were carried out according to a published method.[18] The spherical $NaGdF_4$:Yb,Er nanocrystals were prepared by the following procedures. In brief, $GdCl_3{\cdot}6H_2O$ (0.297 g, 0.8 mmol), $YbCl_3{\cdot}6H_2O$ (0.070 g, 0.18 mmol), and $ErCl_3{\cdot}6H_2O$ (0.008 g, 0.02 mmol) were mixed with 14 mL OA and 16 mL ODE in a 100 mL flask. Then the resultant mixture was heated to 150 °C under nitrogen protection to form a homogeneous solution. After the solution was cooled down to 50 °C, 10 mL methanol solution containing NaOH (0.100 g, 2.5 mmol) and NH_4F (0.148 g, 4 mmol) was slowly introduced. The reaction mixture was kept under stirring for 30 min, then methanol in the system was removed under reduced pressure at 100 °C. The finally formed reaction mixture was heated to 300 °C under nitrogen protection. The reaction was allowed for 30 min and then terminated by cooling the mixture to room temperature. The nanoparticles were precipitated by ethanol, collected by centrifugation, and washed with ethanol several times, before being redispersed in cyclohexane. The rod-shape $NaYF_4$:Yb,Er nanocrystals were synthesized in a similar way except that 0.8 mmol $GdCl_3{\cdot}6H_2O$ was replaced by 0.5 mmol $YCl_3{\cdot}6H_2O$.

Characterization: TEM images and SAED patterns were obtained using a JEM-100CXII microscope operating at 100 kV for characterizing the particle size, shape, and crystalline structure. HRTEM images and SAED patterns were obtained using a JEOL 2010 microscope operating at 200 kV (200 pA cm^{-2}) for monitoring the time dependent changes of nanocrystals. All SAED patterns were compared for identification by JCPDS cards. Specifically: $NaGdF_4$ (No. 27–0699); GdF_3 (No. 05–0747); $NaYF_4$ (No. 16–0334); and YF_3 (No. 05–0546). Energy dispersive X-ray (EDX) analysis was performed under 200 kV accelerating voltage to investigate the composition of the nanocrystal before and after being subjected to 200 kV electron beam irradiation with a current density up to 200 pA cm^{-2} for 10 min. The beam size for EDX measurements was 1.5 nm. The integration time was 60 s. Point-by-point EDX analysis of nanocrystals was taken across individual particles to investigate the compositional changes of the $NaREF_4$ nanocrystals after irradiation.

Modelling: Autodesk 3ds Max 2014 software was used for the modelling of nanocrystal morphology. The particle models were built up by randomly fitting small spheres with a transparency of 70% to simulate density contrast for comparing with the TEM results.

Supporting Information

Supporting Information is available from the Wiley Online Library or from the author.

Acknowledgements

X.S., B.W., and I.K. contributed equally to this paper. The authors thank the National Basic Research Program of China (2011CB935800), NSFC (81090271, 21203211, 21021003), CAS (CMS-PY-201309, CMS-PY-201314), and CAS visiting fellowship (2013Y2JA0003).

[1] M. J. Yacaman, C. Gutierrez-Wing, M. Miki, D. Yang, K. Piyakis, E. Sacher, *J. Phys. Chem. B* **2005**, *109*, 9703.
[2] A. H. Latham, M. J. Wilson, P. Schiffer, M. E. Williams, *J. Am. Chem. Soc.* **2006**, *128*, 12632.
[3] X. Zhu, J. Su, Y. Wu, L. Wang, Z. Wang, *Nanoscale* **2014**, *6*, 1499.
[4] M. Gao, X. Zhang, B. Yang, J. Shen, *J. Chem. Soc.* **1994**, 2229.
[5] A. Krasheninnikov, F. Banhart, *Nat. Mater.* **2007**, *6*, 723.
[6] S. Wu, F. Cao, H. Zheng, H. Sheng, C. Liu, Y. Liu, D. Zhao, J. Wang, *Appl. Phys. Lett.* **2013**, *103*, 243101.
[7] R. Csencsits, R. Gronsky, *Ultramicroscopy* **1987**, *23*, 421.
[8] J. Reyes-Gasga, R. Garcia-Garcia, E. Brès, *Phys. B* **2009**, *404*, 1867.
[9] W. Xu, Y. Zhang, G. Cheng, W. Jian, P. C. Millett, C. C. Koch, S. N. Mathaudhu, Y. Zhu, *Nat. Commun.* **2013**, *4*.
[10] D. Ferrer, D. A. Blom, L. F. Allard, S. Mejía, E. Pérez-Tijerina, M. José-Yacamán, *J. Mater. Chem.* **2008**, *18*, 2442.
[11] Y. Tang, M. Ouyang, *Nat. Mater.* **2007**, *6*, 754.
[12] W. Huang, W. Qian, M. A. El-Sayed, Y. Ding, Z. L. Wang, *J. Phys. Chem. C* **2007**, *111*, 10751.
[13] B. K. Canfield, S. Kujala, K. Laiho, K. Jefimovs, J. Turunen, M. Kauranen, *Opt. Express* **2006**, *14*, 950.
[14] S. Zhou, K. Potzger, K. Kuepper, J. Grenzer, M. Helm, J. Fassbender, E. Arenholz, J. Denlinger, *J. Appl. Phys.* **2008**, *103*, 043901.
[15] G. V. Hartland, *Nat. Mater.* **2007**, *6*, 716.
[16] F. Banhart, *Rep. Prog. Phys.* **1999**, *62*, 1181.
[17] P. R. Diamente, M. Raudsepp, F. C. van Veggel, *Adv. Funct. Mater.* **2007**, *17*, 363.
[18] C. Liu, Z. Gao, J. Zeng, Y. Hou, F. Fang, Y. Li, R. Qiao, L. Shen, H. Lei, W. Yang, M. Gao, *ACS Nano* **2013**, *7*, 7227.
[19] Z. Xu, C. Li, P. Yang, C. Zhang, S. Huang, J. Lin, *Cryst. Growth Des.* **2009**, *9*, 4752.
[20] S. Gai, G. Yang, X. Li, C. Li, Y. Dai, F. He, P. Yang, *Dalton Trans.* **2012**, *41*, 11716.

[21] S. Gai, C. Li, P. Yang, J. Lin, *Chem. Rev.* **2013**.
[22] P. Yang, S. Gai, J. Lin, *Chem. Soc. Rev.* **2012**, *41*, 3679.
[23] D. Yang, Y. Dai, P. Ma, X. Kang, Z. Cheng, C. Li, J. Lin, *Chem Eur. J.* **2013**, *19*, 2685.
[24] W. Feng, L. D. Sun, Y. W. Zhang, C. H. Yan, *Small* **2009**, *5*, 2057.
[25] L. Glasser, H. D. B. Jenkins, *J. Am. Chem. Soc.* **2000**, *122*, 632.
[26] C. Dong, M. Raudsepp, F. C. van Veggel, *J. Phys. Chem. C* **2008**, *113*, 472.
[27] C. M. Wang, D. R. Baer, J. E. Amonette, M. H. Engelhard, J. Antony, Y. Qiang, *Ultramicroscopy* **2007**, *108*, 43.
[28] S. Xiong, W. Qi, Y. Cheng, B. Huang, M. Wang, Y. Li, *Phys. Chem. Chem. Phys.* **2011**, *13*, 10648.

Received: April 21, 2014
Revised: May 8, 2014
Published online: June 20, 2014

